doi:10.1093/brain/awp102 Brain 2009: 132; 1866–1881 | 1866

BRAIN
A JOURNAL OF NEUROLOGY

Cortical spreading ischaemia is a novel process involved in ischaemic damage in patients with aneurysmal subarachnoid haemorrhage

Jens P. Dreier,[1,2,3] Sebastian Major,[1,2,3] Andrew Manning,[4] Johannes Woitzik,[3,5] Chistoph Drenckhahn,[1,2,3] Jens Steinbrink,[3] Christos Tolias,[4] Ana I. Oliveira-Ferreira,[1,3] Martin Fabricius,[6] Jed A. Hartings,[7] Peter Vajkoczy,[3,5] Martin Lauritzen,[6] Ulrich Dirnagl,[1,3] Georg Bohner,[3,8] Anthony J. Strong[4], for the COSBID study group

1 Department of Experimental Neurology, Charité University Medicine Berlin, Berlin, Germany
2 Department of Neurology, Charité University Medicine Berlin, Berlin, Germany
3 Center for Stroke Research Berlin, Charité University Medicine Berlin, Berlin, Germany
4 Department of Clinical Neuroscience, King's College London, London, UK
5 Department of Neurosurgery, Charité University Medicine Berlin, Berlin, Germany
6 Department of Clinical Neurophysiology, Glostrup Hospital, University of Copenhagen, Copenhagen, Denmark
7 Department of Neurosurgery, University of Cincinnati, Cincinnati, OH, USA
8 Department of Neuroradiology, Charité University Medicine Berlin, Berlin, Germany

Correspondence to: Jens P. Dreier,
Center for Stroke Research Berlin,
Charité Campus Mitte,
Charité University Medicine Berlin,
Charitépl. 1, 10117 Berlin,
Germany
E-mail: jens.dreier@charite.de

The term cortical spreading depolarization (CSD) describes a wave of mass neuronal depolarization associated with net influx of cations and water. Clusters of prolonged CSDs were measured time-locked to progressive ischaemic damage in human cortex. CSD induces tone alterations in resistance vessels, causing either transient hyperperfusion (physiological haemodynamic response) in healthy tissue; or hypoperfusion [inverse haemodynamic response = cortical spreading ischaemia (CSI)] in tissue at risk for progressive damage, which has so far only been shown experimentally. Here, we performed a prospective, multicentre study in 13 patients with aneurysmal subarachnoid haemorrhage, using novel subdural opto-electrode technology for simultaneous laser-Doppler flowmetry (LDF) and direct current-electrocorticography, combined with measurements of tissue partial pressure of oxygen ($ptiO_2$). Regional cerebral blood flow and electrocorticography were simultaneously recorded in 417 CSDs. Isolated CSDs occurred in 12 patients and were associated with either physiological, absent or inverse haemodynamic responses. Whereas the physiological haemodynamic response caused tissue hyperoxia, the inverse response led to tissue hypoxia. Clusters of prolonged CSDs were measured in five patients in close proximity to structural brain damage as assessed by neuroimaging. Clusters were associated with CSD-induced spreading hypoperfusions, which were significantly longer in duration (up to 144 min) than those of isolated CSDs. Thus, oxygen depletion caused by the inverse haemodynamic response may contribute to the establishment of clusters of prolonged CSDs and lesion progression. Combined electrocorticography and perfusion monitoring also revealed a characteristic vascular signature that might be used for non-invasive detection of CSD. Low-frequency vascular fluctuations (LF-VF) ($f < 0.1$ Hz), detectable by functional imaging methods, are determined by the brain's

Received December 30, 2008. Revised March 10, 2009. Accepted March 27, 2009. Advance Access publication May 6, 2009

resting neuronal activity. CSD provides a depolarization block of the resting activity, recorded electrophysiologically as spreading depression of high-frequency-electrocorticography activity. Accordingly, we observed a spreading suppression of LF-VF, which accompanied spreading depression of high-frequency-electrocorticography activity, independently of whether CSD was associated with a physiological, absent or inverse haemodynamic response. Spreading suppressions of LF-VF thus allow the differentiation of progressive ischaemia and repair phases in a fashion similar to that shown previously for spreading depressions of high-frequency-electrocorticography activity. In conclusion, it is suggested that (i) CSI is a novel human disease mechanism associated with lesion development and a potential target for therapeutic intervention in stroke; and that (ii) prolonged spreading suppressions of LF-VF are a novel 'functional marker' for progressive ischaemia.

Keywords: CSI; subarachnoid haemorrhage; cortical spreading depression; neurovascular coupling; default mode

Abbreviations: aSAH = aneurysmal subarachnoid haemorrhage; BOLD = blood oxygen level dependent; COSBID = Cooperative Study on Brain Injury Depolarizations; CSD = cortical spreading depolarization; CSI = cortical spreading ischaemia; CT = computed tomography; DC = direct current; DSA = digital subtraction angiography; ECoG = electrocorticography; GCS = Glasgow Coma Score; HF-ECoG = high-frequency electrocorticogram; HF-VF = high-frequency vascular fluctuations; ICP = intracranial pressure; LDF = laser-Doppler flowmetry; LF-VF = low-frequency vascular fluctuations; MCA = middle cerebral artery; MRI = magnetic resonance imaging; MRS = Modified Rankin Scale; NMDA = *N*-methyl-D-aspartate; $ptiO_2$ = tissue partial pressure of oxygen; rCBF = regional cerebral blood flow; SPC = slow potential change; TCD = transcranial Doppler-sonography; WFNS = World Federation of Neurological Surgeons.

Introduction

The term 'cortical spreading depolarization' (CSD) describes the wave of near-complete neuronal depolarization and neuronal swelling in the brain that is ignited when passive cation influx across the cellular membranes exceeds ATP-dependent sodium and calcium pump activity. The cation influx is followed by water influx and shrinkage of the extracellular space by ~70% (Kraig and Nicholson, 1978; Somjen, 2004). If the normal ion homoeostasis is not restored through additional recruitment of sodium and calcium pump activity, the cell swelling is maintained—a process then termed 'cytotoxic oedema' (Klatzo, 1987) since it potentially leads to cell death through the protracted intracellular calcium surge and mitochondrial depolarization.

Although the ignition of CSD occurs passively, driven by electrical and diffusion forces, energy consumption paradoxically increases since sodium and calcium pumps are immediately activated to correct the intracellular sodium and calcium surge. Thus, even in healthy tissue where CSD is fully reversible, ATP immediately falls by ~50% (Mies and Paschen, 1984). In order to increase oxygen and glucose availability, CSD induces dilatation of resistance vessels in healthy tissue. Hence, regional cerebral blood flow increases during the neuronal depolarization phase. Only after the neuronal repolarization, the phase of vasodilatation is followed by mild vasoconstriction resulting in spreading oligaemia (Lauritzen, 1994).

The opposite of this physiological haemodynamic response to CSD is termed here the inverse haemodynamic response, and occurs when there is local dysfunction of the microvasculature. With the inverse response, severe microvascular spasm instead of vasodilatation is coupled to the neuronal depolarization phase (Dreier *et al*., 1998; Shin *et al*., 2006). The resulting spreading perfusion deficit in turn prolongs the neuronal depolarization [as reflected by a prolonged negative shift of the extracellular direct current (DC) potential] and the intracellular sodium and calcium surge, since the oxygen-/glucose deprivation further reduces ATP availability (Dreier *et al*., 1998, 2002; Sukhotinsky *et al*., 2008). Thus, in animal experiments, a prolonged negative cortical DC shift, the defining electrophysiologic feature for the inverse haemodynamic response, indicates that the hypoperfusion is significant enough to produce a mismatch between neuronal energy demand and supply (Dreier *et al*., 1998, 2000, 2002; Sukhotinsky *et al*., 2008). Accordingly, the term 'cortical spreading ischaemia' (CSI) describes the CSD-induced perfusion deficit when it leads to a prolonged negative cortical DC shift (Dreier *et al*., 1998, 2002).

In the presence of normal baseline perfusion, very prolonged, pharmacologically induced CSI is sufficient to produce widespread focal necrosis (Dreier *et al*., 2000). This suggested that the inverse haemodynamic response to CSD is: (i) a process by which CSD increases the likelihood of inducing cell death and; thus, (ii) is a promising target for therapeutic intervention (Dreier *et al*., 1998, 2000). CSI has been observed in a rat model replicating conditions following aneurysmal subarachnoid haemorrhage (aSAH) (Dreier *et al*., 1998), in rat models of hypotension and hypoxia (Sukhotinsky *et al*., 2008), as well as in the penumbra after middle cerebral artery (MCA) occlusion in mice and cats (Shin *et al*., 2006; Strong *et al*., 2007).

Here, we investigated whether the full spectrum from physiological to inverse haemodynamic responses occurs in the diseased human brain in a fashion similar to that seen in animals. Moreover, we studied whether CSD can be identified by a vascular signal that is independent of the perfusion change. For these purposes, small optodes were integrated into subdural electrode strips that allowed the simultaneous measurement of the electrocorticogram (ECoG) with regional cerebral blood flow using laser-Doppler flowmetry (LDF) in aSAH patients. Thus, the local haemodynamic response to CSD was recorded at given optoelectrode pairs on the surface of the human brain with high-spatial and temporal resolution.

aSAH patients were studied since animal experiments suggested a role for CSI in delayed ischaemia (Dreier *et al*., 1998). Moreover,

delayed ischaemic stroke after aSAH is a model disease for ischaemic stroke and future intervention trials for two reasons. First, it is the most important in-hospital complication after aSAH with a peak occurrence around day 7, while the patient is already on the intensive care unit (MacDonald *et al*., 2007). Neuroprotectants have been shown to be most effective when given either before, or within minutes after, the onset of acute neuronal injury. Thus, delayed stroke allows administration of a neuroprotectant prior to the possible insult, or very shortly thereafter, to prove or disprove the concept. Second, neurosurgical procedures are indicated early after the initial haemorrhage and allow placement of invasive probes. This provides the unique option to monitor invasively the whole period of ischaemic stroke development.

Materials and Methods

Patient recruitment and clinical care

Thirteen patients with major aSAH were recruited by four centres of the Cooperative Study on Brain Injury Depolarizations (COSBID, see www.cosbid.org): Campus Charité Mitte Berlin ($n = 9$), Campus Benjamin Franklin Berlin ($n = 2$), King's College London ($n = 1$), and Glostrup Hospital Copenhagen ($n = 1$). The research protocol was approved by the local ethics committees. Clinical and research consents were obtained according to the Declaration of Helsinki after a clinical decision had been taken to offer surgical treatment. aSAH was diagnosed by assessment of CT scans. Haemorrhage was graded according to the Fisher scale, and clinical presentation according to the World Federation of Neurological Surgeons (WFNS) scale. The indications for neurosurgical treatment are given in Table 1. Surgery allowed the placement of a single, linear, 6-contact (platinum) electrocorticography recording strip (Wyler, 5-mm diameter; Ad-Tech Medical, Racine, Wisconsin, USA) on cortex accessible through the craniotomy or via an extended burr-hole (Dreier *et al*., 2006; Fabricius *et al*., 2006). Four optodes neighbouring electrodes 3–6 were integrated in the recording strip for LDF (Perimed AB, Järfälla, Sweden). After surgery, patients were transferred to the intensive care unit. Intracranial pressure (ICP) was monitored via ventricular drainage catheter in 12 of the 13 patients. Glasgow Coma Score (GCS), blood gases, glucose and electrolytes were documented every 6 h. A thorough neurological examination was performed at least daily. Serial CT scans were performed postoperatively at the time of clinical deterioration and after the monitoring period to screen for delayed infarcts. Vasospasm was defined using digital subtraction angiography (DSA) as >30% narrowing of the arterial luminal diameter in one of the following arterial segments: A1, A2, M1, M2 and C1–C2. Magnification errors were corrected by comparing extradural segments of the internal carotid artery (C4–C5). Using transcranial Doppler-sonography (TCD), significant vasospasm was defined by a mean velocity >200 cm/s in at least one MCA and vasospasm was excluded if the MCA mean velocities remained below 120 cm/s throughout the observation period. Patients with delayed ischaemia were treated with triple-H therapy (hypertension, hypervolaemia and haemodilution) as described previously (Dreier *et al*., 2006). Oral nimodipine was given prophylactically in all patients with aSAH.

Electrocorticography and LDF using subdural opto-electrode strips

Electrocorticography recordings were acquired continuously in five active channels from the 6-electrode (linear array) subdural strips. Electrode 1 served as ground, while electrodes 2–6 (interelectrode distance 1 cm) were connected in sequential unipolar fashion to a GT205 amplifier (0.01–50 Hz) (ADInstruments, New South Wales, Australia), each referenced to an ipsilateral subgaleal platinum electrode. The DC-electrocorticography was additionally recorded using a BrainAmp amplifier (0–50 Hz) (BrainProducts GmbH, Munich). Data were sampled at 200 Hz and recorded and reviewed with the use of a Powerlab 16/SP analog/digital converter, Chart-5 software (ADInstruments, New South Wales, Australia) and BrainVision Recorder software (BrainProducts GmbH, Munich), respectively. The tissue partial pressure of oxygen ($ptiO_2$) was recorded in eight patients using an intraparenchymal oxygen sensor (Licox, Integra Lifesciences Corporation, Plainsboro, NJ, USA).

Data analysis

CSD was defined by the sequential onset in adjacent channels of a propagating slow potential change (SPC) (Fabricius *et al*., 2006). The parallel high-frequency-electrocorticography depression was *a priori* defined by a rapidly developing reduction of the power of the electrocorticogram (ECoG) amplitude by at least 50%. The duration of the depression period of the high-frequency-electrocorticography activity was measured as the interval between depression onset and onset of restoration of activity using the integral of power of the band-pass filtered activity (time constant decay, 60 s) as described previously (Dreier *et al*., 2006).

The high-frequency-electrocorticography was split into different frequency bands roughly according to classically defined electroencephalographic conventions (Leopold *et al*., 2003) comprising the following ranges: sub-δ (0.5–1 Hz), δ (1–4 Hz), θ (5–8 Hz), α (9–14 Hz), β (15–30 Hz) and γ_L (30–50 Hz). Regional cerebral blood flow was simultaneously recorded in the full-band between 0 and 10 Hz using LDF. The full-band of the regional cerebral blood flow signal is dominated by baseline changes in the frequency range from 0 to 0.05 Hz on which low-frequency vascular fluctuations (LF-VF) (0.05–0.1 Hz) and high-frequency vascular fluctuations (HF-VF) (0.5–10 Hz) are superimposed. As demonstrated in Fig. 1, the HF-VF are dominated by the microcirculatory pulse since they are coherent with the systemic arterial pressure variations as recorded invasively in the radial artery ($n = 7$ patients).

For the analysis of isolated CSD, the curves were first screened for recording periods containing CSDs with at most minor artefacts. Then, the isolated CSD of each patient was selected with the longest depression period of the high-frequency-electrocorticogram (HF-ECoG) activity, since the study focused on the consequences of energy compromise and it is assumed that a prolonged duration of the HF-ECoG depression is an indicator of energy depletion in the animal and human brain (Nedergaard and Hansen, 1993; Back *et al*., 1994; Dreier *et al*., 2006; Fabricius *et al*., 2006). Thereafter, the opto-electrode pair was taken for analysis that demonstrated a large SPC indicating appropriate positioning of this particular electrode on the cortex and a regional cerebral blood flow signal with well-expressed HF-VF (pulse). This procedure resulted in 12 recordings of an isolated CSD for the statistical comparison. Data are given as median (first, third quartile). The statistical tests used are specified in the text.

Table 1 Summary of demographic and treatment-related data

No	Age (years), sex	WFNS grade	Fisher grade	Location of aneurysm	Significant proximal vasospasm	Delayed CT- or MRI-proven infarct	Surgical intervention	Location of electrode strip	Start of ECoG monitoring (day after insult)	Duration of ECoG monitoring (h)	Duration of rCBF monitoring (h)	Total number of CSDs	Total duration of depressed ECoG (minutes)	Day of analysed CSD cluster	Day of analysed isolated CSD	Sedation during analysed events	MRS on Day 14
1	62, F	5	3	AcoP	Y	Cortex/ subcortical	Placement of oxygen sensor	Fronto-parietal cortex (compare Fig. 7)	3	208	158	20	4188.0	9	—	Midazolam/ ketamine	6
2	69, F	4	3	AcoP	—	Cortex/ sub-cortical	Evacuation of subdural and temporal intracerebral haematoma	Fronto-parietal cortex distantly of intracerebral haematoma	1	94	94	60	743.1	4	3	N	6
3	57, M	1	3	MCA	Y	N	Aneurysm clipping	Adjacent to cortex over 6 × 4 cm fronto-temporal intracere-bral haematoma	1	208	47	27	624.3	2	2	Mida-zolam	5
4	71, M	5	4	AcoA	N	N	Aneurysm clipping	Adjacent to cortex over a 6 × 2 cm frontal intracerebral haematoma	1	248	248	64	2800.8	4	2	N	5
5	51, F	5	3	MCA	Y	N	**Aneurysm clipping**	Adjacent to cortex over a 6 × 1 cm frontoparietal intracerebral haematoma	0	201	143	26	656.2	0	1	Mida-zolam	5
6	70, F	1	3	PericA	N	Subcortical	Aneurysm clipping	Frontolateral base	0	60	60	3	25.1	—	1	N	5
7	56, F	4	3	MCA	N	Subcortical	Aneurysm clipping	Frontolateral base	1	183	183	2	13.0	—	6	Midazolam/ thio-pental	5
8	38, M	5	3	AcoA	Y	N	Aneurysm clipping	Frontolateral base	0	153	112	15	522.8	—	7	Methohexital	5
9	48, M	4	3	MCA	N	N	**Aneurysm clipping**	Frontolateral base	1	238	217	31	395.8	—	1	Mida-zolam	5
10	47, F	5	3	MCA	N	N	**Aneurysm clipping**	Frontolateral base	1	132	132	70	1915	—	4	Midazolam	0
11	47, M	4	3	ACoA	Y	N	**Aneurysm clipping**	Frontolateral base	1	281	281	51	715.8	—	10	Midazolam	5
12	56, F	4	3	MCA	N	N	**Aneurysm clipping**	Frontolateral base	1	287	104	189	1561.5	—	5	N	0
13	60, F	2	3	ICA	—	N	**Aneurysm clipping**	**Frontolateral base**	1	174	174	45	335.8	—	2	Propofol	4

WFNS = World Federation of Neurological Surgeons scale; ECoG = electrocorticogram; rCBF = regional cerebral blood flow, MRS = Modified Rankin Scale; AcoA = anterior communicating artery, AcoP = posterior communicating artery, PeriC = pericallosal artery.

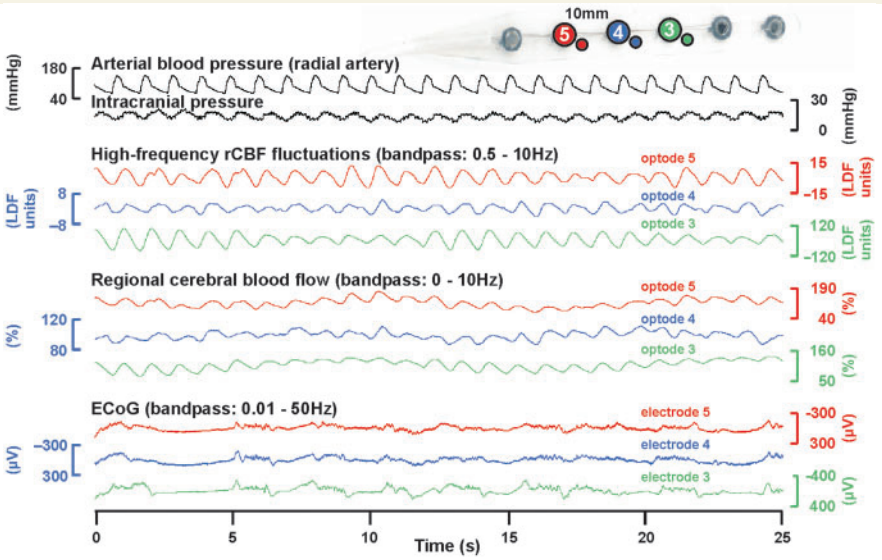

Figure 1 Obvious coherences (i) between high-frequency-ECoG activities at different electrodes, (ii) between LF-VF at different optodes and (iii) between HF-VF, arterial pulse and intracranial pressure fluctuations. The ECoG shows a burst suppression pattern (Case 10).

Eight of the 12 patients were sedated and 10 were ventilated during the single CSD taken for analysis. Thus, the recorded GCS was only 3 (3, 6), which probably underestimated the clinical status that would have been observed without sedation. The following vital signs and paraclinical parameters were documented during the CSD ($n = 12$): temperature [37.2 (36.3, 37.7)°C], mean arterial pressure [96 (93, 98) mmHg], intracranial pressure [17 (16, 18) mmHg], cerebral perfusion pressure [78 (74, 82) mmHg], pH [7.44 (7.42, 7.44)], pCO_2 [39.0 (35.3, 41.8) mmHg], oxygen saturation [98.5 (97.9, 99.2)%], serum glucose [120 (107, 148) mg/dl], serum lactate [7 (6, 9) mg/dl], haematocrit [29.5 (28.9, 32.2)%], serum sodium [143 (140, 147) mmol/l] and serum potassium [4.2 (3.7, 4.3) mmol/l]. Eight of 12 patients received noradrenaline intravenously [median dose: 0.11 (0.07, 0.22) µg/kg BW/min]. Continuous recordings of intracranial pressure and arterial pressure were performed in seven patients without significant change during the CSD. The resting ECoG activity was characterized by a burst suppression pattern in six cases and dominated by sub-δ- in 3, δ- in 2 and θ-activity in one case [median peak to peak amplitude of resting ECoG activity: 368 (256, 409) µV].

Limitations of the set-up

We applied the combination of DC-ECoG and LDF technology, hitherto used only in experimental animals. This combination represents the gold standard for identification of the physiological and inverse haemodynamic responses to CSD in animals (Dreier *et al*., 1998). The choice of the opto-electrode strip was justified since: (i) no modification of the surgical procedure was necessary compared to a recording strip without optodes; (ii) the use of a single, narrow linear electrode strip allowed withdrawal at the bedside; (iii) no infectious or haemorrhagic complications were encountered and (iv) the use of the opto-electrode strips clearly allowed identification of physiological and inverse haemodynamic responses to CSD, respectively. However, there were some limitations compared with animal experiments. The optodes were more delicate, the monitoring period was significantly longer, and the nursing procedures required in intensive care necessarily involve patient movement. Therefore, even with great care, breaks of the fine light fibres may occur. Furthermore, the opto-electrode pairs cannot be placed over regions of interest under visual control. Therefore, in most patients only one or two of the four optodes yielded a stable signal of sufficient quality. Moreover, during continuous monitoring over days, movement artefacts produce baseline shifts, and a zero flow value cannot be obtained in a living human being. Therefore, changes of regional cerebral blood flow during CSD were only calculated in relation to regional cerebral blood flow immediately before CSD and only the pattern of regional cerebral blood flow changes was assessed. LDF and ECoG were closely adjacent but not recorded at exactly the same site, thus limiting the precision of temporal correlations between the two.

Results

Table 1 gives a summary of the clinical and monitoring characteristics of the 13 patients studied. CSD occurring in temporal clusters and in isolation were analysed separately (see Materials and Methods section). Twelve patients showed isolated CSDs, which were characterized by a SPC of 3.4 (1.9, 5.3) mV (high-pass filter with lower frequency limit: 0.01 Hz). The 'true' DC potential (lower frequency limit: 0 Hz) was measured in eight patients during isolated CSDs [negative shift: –10.8 (–9,7, –13,7) mV; duration: 153 (123, 283) s]. CSD propagation velocity was 2.1 (1.8, 2.9) mm/min assuming an ideal linear spread along the recording strip. Figure 2A gives an original recording of a negative DC shift associated with CSD propagating from opto-electrode 6–4 at a velocity of 1.9 mm/min. Note the remarkable similarity of the negative DC shift (–19 mV at electrode 6) to animal findings (Lauritzen, 1994). Figure 2B allows a direct comparison between the 'true' negative DC shift (1) and its distorted manifestation as a smaller SPC in recordings with a lower frequency limit of 0.01 Hz (Trace 2).

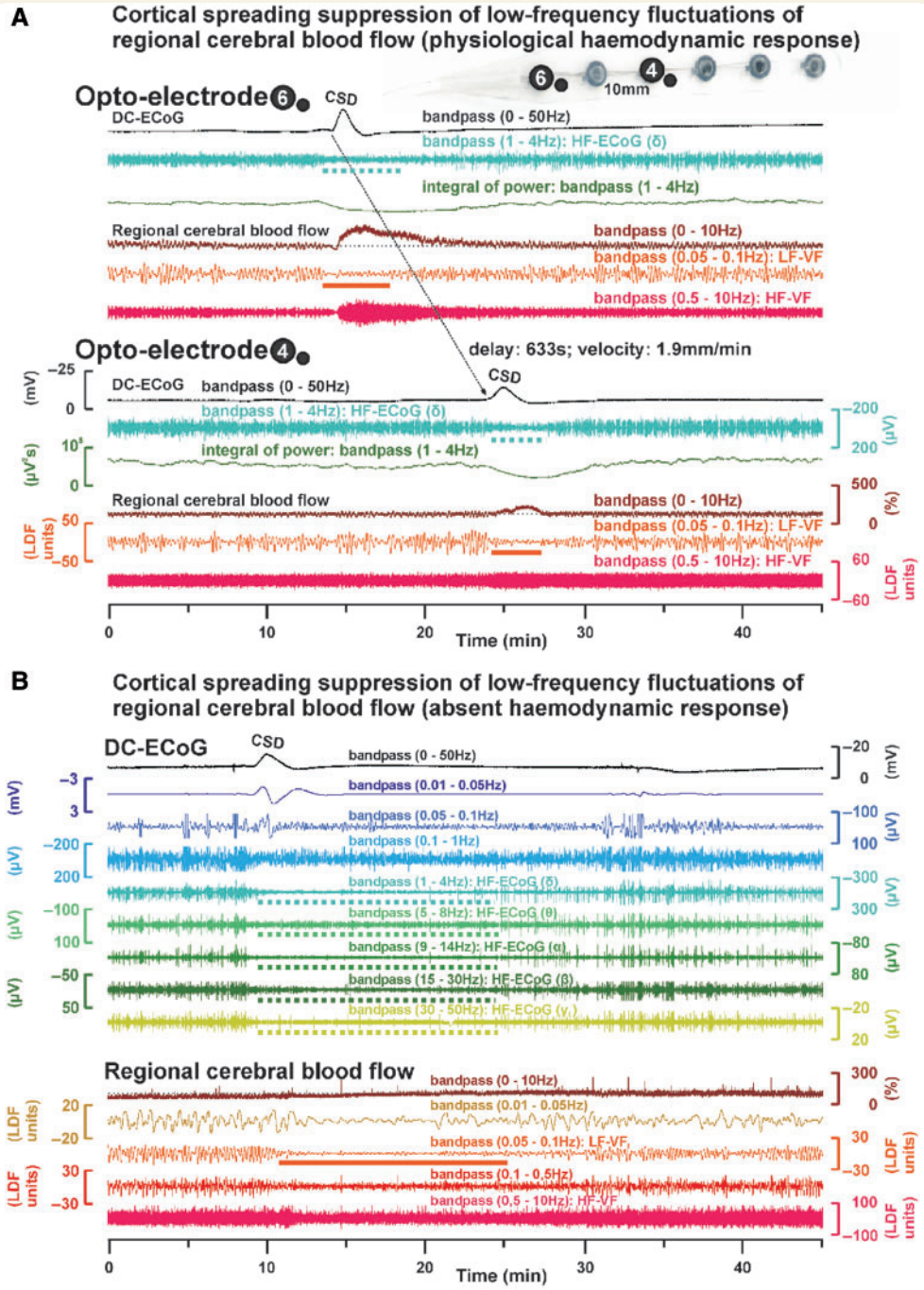

Figure 2 Spreading depression of high-frequency-ECoG activity and spreading suppression of LF-VF correlate in the human brain during physiological and absent haemodynamic responses to CSD, respectively. (**A**) On the upper right, the opto-electrode strip is shown. The 12 traces represent simultaneous recordings of a single CSD (Case 7) that propagated from opto-electrode 6 (Traces 1–6) to 4 (Traces 7–12). The calibration bars at opto-electrode 4 (Traces 7–12) also apply to the corresponding traces at opto-electrode 6 (Traces 1–6). Opto-electrode 6: the first three traces identify the CSD electrophysiologically. Trace 1 (black): full-band ECoG changes including the negative DC potential; Trace 2 (light blue): depression of high-frequency-ECoG activity (δ-band); Trace 3 (green): integral of power of the δ-band, used to calculate the depression period. Trace 4 (brown) (full-band regional cerebral blood flow signal): displays a flow increase characteristic of the physiological haemodynamic response to CSD. LF-VF (0.05–0.1 Hz) and HF-VF (0.5–10 Hz) are contained in the full-band regional cerebral blood flow signal. During CSD, the LF-VF (Trace 5) became suppressed, while the HF-VF (Trace 6) increased underscoring their differential nature (HF-VF = pulse). Note that the LF-VF recovery (Trace 5) starts at a similar moment as the recovery of the high-frequency-ECoG (Trace 2). Opto-electrode 4: the CSD spread from opto-electrode 6–4 at a rate of 1.9 mm/min. The changes at opto-electrode 4 are similar to those at opto-electrode 6. Importantly, note simultaneous propagation of the spreading suppression of LF-VF and the spreading depression of high-frequency-ECoG. (**B**) The 14 traces represent simultaneous recordings of a single CSD (Case 3) at opto-electrode 5. The nine traces of the upper part identify the CSD

Isolated CSDs can be associated with physiological or absent haemodynamic responses

Four of the 12 isolated CSDs analysed were rated to display a physiological haemodynamic response, since the initial response was predominantly hyperaemic. Hyperaemia reached a level of 257 (211, 311)% lasting for 689 (512, 812) s followed by spreading relative oligaemia to 92 (79, 102)%. The SPC preceded the initial spreading hyperaemia by 47 (37, 235) s. Figure 2A demonstrates an original recording of an isolated CSD with physiological haemodynamic response (Case 7). Another three of the 12 CSDs did not show any significant change in level of regional cerebral blood flow at all. This behaviour was rated as absent haemodynamic response (Case 3, Fig. 2B).

Isolated CSDs can be associated with inverse haemodynamic responses

Figure 3A shows an example of the inverse haemodynamic response to CSD (Case 8) which was observed in the remaining 5 of 12 isolated CSDs. Based on previous experimental work, the following observations characterized this inverse response or CSI: (i) The DC potential change preceded the initial hypoperfusion by 65 (16, 83) s; (ii) the local hypoperfusion was characterized by a fall of regional cerebral blood flow to 59 (31, 62)% lasting for 118 (88, 265) s that did not start in a step-like fashion as in a cardiac arrest or embolic occlusion, but rather gradually reached the trough within 90 s; (iii) the local hypoperfusion propagated with the cortical DC potential negativity in the tissue at a rate of 3.5 (1.6, 3.5) mm/min (in Fig. 3A propagation from opto-electrode 3–5 is shown); (iv) including all eight CSDs with simultaneous recordings of regional cerebral blood flow and DC potential, linear regression found that the durations of the initial hypoperfusion and the cortical DC potential negativity were highly significantly correlated [Fig. 3B, $R = 0.92$, $P < 0.001$, $n = 8$, compare Dreier *et al*. (2002) and Sukhotinsky *et al*. (2008) for this linear regression in rat recordings]; (v) moreover, linear regression demonstrated that the durations of the cortical DC potential negativity and the energy-dependent recovery of the HF-ECoG activity were highly correlated (Fig. 3C, $R = 0.93$, $P < 0.001$, $n = 8$); finally (vi) linear regression demonstrated a highly significant correlation between initial changes in level of regional cerebral blood flow and $ptiO_2$ in response to CSD (Fig. 4D, $R = 0.84$, $P = 0.019$, $n = 7$). Figure 4A gives an example of spreading hyperoxia (arrows) associated with a physiological haemodynamic response to CSD. Figure 4B shows spreading hypoxia (arrows) associated with an inverse haemodynamic response to CSD, supporting the hypothesis that CSI leads to significant reduction of energy substrate availability. Figure 4C shows an epileptic seizure associated with physiological haemodynamic response and hyperoxia (arrow) for comparison.

Spreading suppressions of low-frequency vascular fluctuations correlate with HF-ECoG depressions, not perfusion changes

Baseline changes in vascular smooth muscle tone of resistance vessels essentially determine the level of local tissue perfusion. LF-VF occur superimposed on the baseline changes in vascular tone and level of perfusion, while HF-VF represent the pulse and are superimposed on the LF-VF (Fig. 1).

We found that LF-VF were suppressed during CSD regardless of the perfusion response. In the case of the physiological haemodynamic response to CSD illustrated in Fig. 2A (Case 7), a spreading suppression of LF-VF (traces 5 and 11, respectively) in both opto-electrode Pairs 6 and 4 was time-locked to the spreading depression of high-frequency-ECoG activity (Traces 2 and 8, respectively). Figure 2B (Case 3) shows an example for the absent haemodynamic response to CSD. Despite the absent perfusion response, the LF-VF became transiently suppressed. Spreading suppression of LF-VF also accompanied spreading depression of high-frequency-ECoG activity during the inverse haemodynamic response to CSD (Fig. 3D).

It has been suggested that LF-VF arise from the resting neuronal activity which is reflected in the high-frequency-ECoG (Biswal *et al*., 1995; Fox and Raichle, 2007). If this hypothesis is correct, then the spreading suppression of LF-VF should correlate with the spreading depression of high-frequency-ECoG induced by CSD.

electrophysiologically. The five traces of the lower part characterize the regional cerebral blood flow response, remarkable for only a very marginal increase of regional cerebral blood flow (absent haemodynamic response to CSD). Upper part: Trace 1 (black): full-band ECoG changes of CSD including DC potential; Traces 2–9 (different shades of blue and green): different frequency bands contained in the full-band signal of Trace 1. The frequency band of 0.01–0.05 Hz (Trace 2) has been used previously to identify the SPC in the human brain (Dreier *et al*., 2006; Fabricius *et al*., 2006). The advantage of the (unfiltered) DC potential over this frequency band is that the duration of the DC negativity is a summary measure that reflects the time period until the energy dependent repolarization. The depression of ECoG activity is best seen in the higher frequency bands [δ (Trace 5), θ (Trace 6), α (Trace 7), β (Trace 8) and γ_L (Trace 9)], whilst it is less obvious in the lower frequency bands (traces 3 and 4). Lower part: Trace 10 (brown) (full-band regional cerebral blood flow signal): displays no significant perfusion change (absent haemodynamic response to CSD). Traces 11–14: different frequency bands contained in the full-band signal of regional cerebral blood flow. Note the strong suppression of the LF-VF (Trace 12, orange) despite the absence of a significant perfusion change in Trace 10. Also note that the durations of the suppression of LF-VF (solid horizontal bar, Trace 12) and the depression of high-frequency-ECoG activity (δ-γ_L frequency bands, broken horizontal bars, Traces 5–9) are similar. Also note that the durations of the depression periods of LF-VF and HF-ECoG are significantly longer in (**B**) (absent haemodynamic response to CSD) compared with (**A**) (physiological haemodynamic response to CSD) consistent with the notion that the recovery of synaptic activity depends on energy supplied by regional cerebral blood flow.

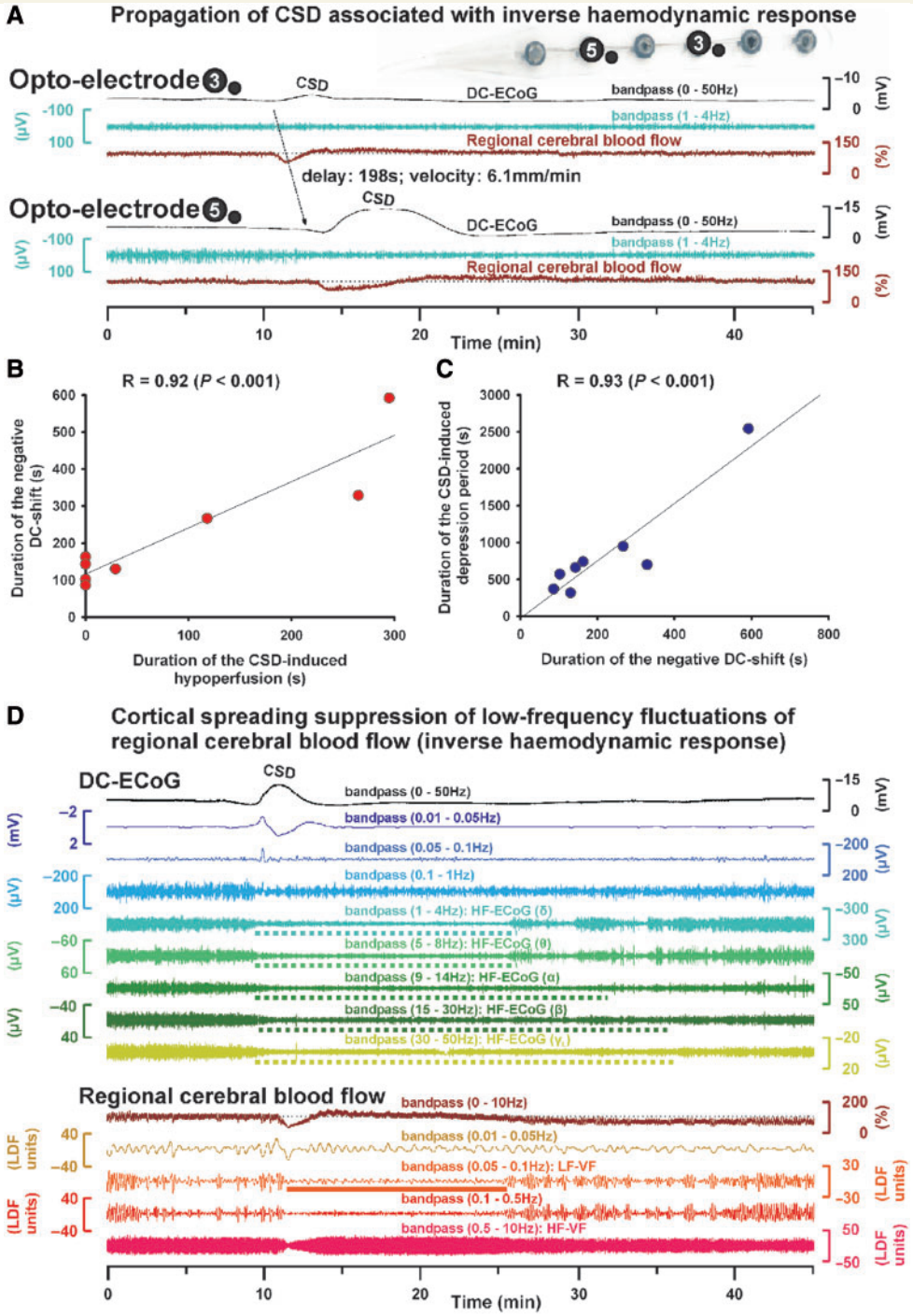

Figure 3 Inverse haemodynamic response to CSD. (**A**) On the upper right, the opto-electrode strip is shown. The six traces represent simultaneous recordings of a single CSD with inverse haemodynamic response (Case 8) that propagated from opto-electrode 3 (Traces 1–3) to 5 (Traces 4–6). Note that the CSD-induced initial hypoperfusion at optode 5 lasts for 4.9 min and is associated with a prolonged negative DC shift lasting for 9.9 min. The prolongation of the direct current negativity renders this hypoperfusion a CSI, meaning that it produces a delay of the energy dependent recovery from the extracellular direct current negativity (reflecting intracellular sodium and calcium surge). Note that the durations of direct current negativity and CSD-induced hypoperfusion are similar at opto-electrode 5 and markedly longer lasting than those at opto-electrode 3. (**B**) Linear regression showing that the durations of initial hypoperfusion and cortical DC negativity are correlated [compare (**A**)]. (**C**) Linear regression showing that the durations of cortical DC potential negativity and energy-dependent recovery of high-frequency-ECoG activity are correlated. (**D**) Fourteen traces showing simultaneous recordings of a single CSD (Case 11) at opto-electrode 3 associated with inverse haemodynamic response. The nine traces of the upper part identify the CSD electrophysiologically similarly as in Fig. 2B. The five traces of the lower part characterize regional cerebral blood flow. The duration of CSI (Trace 10, brown) was 2 min, the duration of the negative DC shift (Trace 1, black) 4.5 min. Note simultaneous long-lasting depression of high-frequency-ECoG activity (broken horizontal bars in Traces 5–9) and suppression of LF-VF (solid horizontal bar in Trace 12, orange).

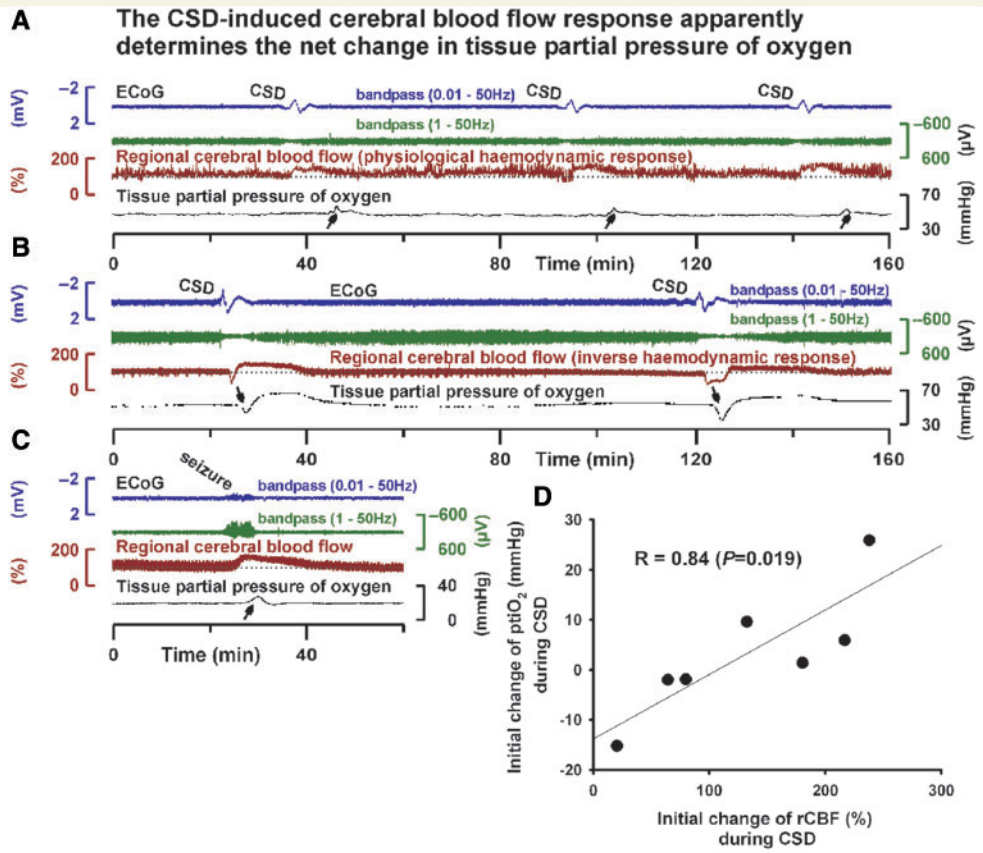

Figure 4 The physiological haemodynamic response to CSD is associated with spreading hyperoxia, whilst the inverse haemodynamic response is associated with spreading hypoxia. (**A**) Three CSDs are shown (Case 12) characterized by a SPC (Trace 1, blue line, lower frequency limit 0.01 Hz), a short-lasting depression of the high-frequency-ECoG activity (Trace 2, green), initial hyperaemia (Trace 3, brown, physiological haemodynamic response to CSD) and tissue hyperoxia (Trace 4, black, arrows). (**B**) Two CSDs are shown (Case 11) characterized by a SPC (Trace 1, blue), a longer-lasting depression of the high-frequency-ECoG activity (Trace 2, green), CSI (Trace 3, brown, inverse haemodynamic response to CSD) and tissue hypoxia (Trace 4, black, arrows). (**C**) A seizure is given (Case 4) with only minor SPC (Trace 1) compared with that of a CSD, rhythmic 4/s δ-activity (amplitude: ~700 μV) (Trace 2), hyperaemia (Trace 3) and hyperoxia (Trace 4, arrow). (**D**) Linear regression showing correlation between the initial changes in level of regional cerebral blood flow and parenchymal $ptiO_2$ in response to CSD.

Isolated CSDs were associated with a significant spreading depression of high-frequency-ECoG activity in the sub-δ, δ-, θ-, α-, β- and γ_L frequency bands, but not in frequencies below 0.5 Hz (Repeated measures ANOVA on ranks with Dunn's *post hoc* test, $n = 12$, $P < 0.05$) (Fig. 5A). For example, the δ-power significantly decreased from 909 (498, 1734) to 195 (86, 575) μV^2 followed by a significant recovery to 920 (473, 1508) μV^2 (Repeated measures ANOVA on ranks with Dunn's *post hoc* test, $n = 12$, $P < 0.05$).

LF-VF (0.05–0.1 Hz) was observed in 10 of 12 cases. The median frequency of the LF-VF was 0.079 (0.070, 0.091) Hz. During CSD, LF-VF became significantly suppressed (Repeated measures ANOVA on ranks with Dunn's *post hoc* test, $n = 10$, $P < 0.05$) (Fig. 5A). The power of the LF-VF robustly and significantly decreased from 128.3 (88.4, 199.2) to 2.8 (2.0, 7.8) LDF U^2 followed by a significant recovery to 99.7 (47.3, 206.2) LDF U^2 after CSD (Repeated measures ANOVA on ranks, $n = 10$, $P < 0.05$). The degree of LF-VF suppression was not significantly different between CSDs with different haemodynamic responses.

No significant difference was detected between the durations of the spreading suppressions of LF-VF [428 (320, 847) s] and high-frequency-ECoG activity [sub-δ: 943 (578, 1290) s, δ: 660 (470, 843) s, θ: 660 (538, 854) s, α: 750 (622, 1030) s, β: 678 (539, 957) s, γ_L: 340 (239, 1069) s, Repeated measures ANOVA on ranks, $n = 7$]. Importantly, the durations of the spreading suppression of LF-VF and spreading depression of high-frequency-ECoG activity correlated significantly [Linear regression with sub-δ ($R = 0.70$, $P = 0.026$, $n = 10$), δ ($R = 0.91$, $P < 0.001$, $n = 10$, Fig. 5B), θ ($R = 0.84$, $P = 0.005$, $n = 9$), α ($R = 0.88$, $P = 0.004$, $n = 8$), β ($R = 0.87$, $P = 0.002$, $n = 9$), γ_L ($R = 0.93$, $P < 0.001$, $n = 8$)].

HF-VF follow the perfusion change

The HF-VF followed changes in perfusion, whether the predominant response to CSD was hyperaemia (Fig. 2A, Traces 6 and 12) or hypoperfusion (Fig. 3D, Trace 14). Including all 12 CSDs, linear regression found that the mean change in power of the HF-VF

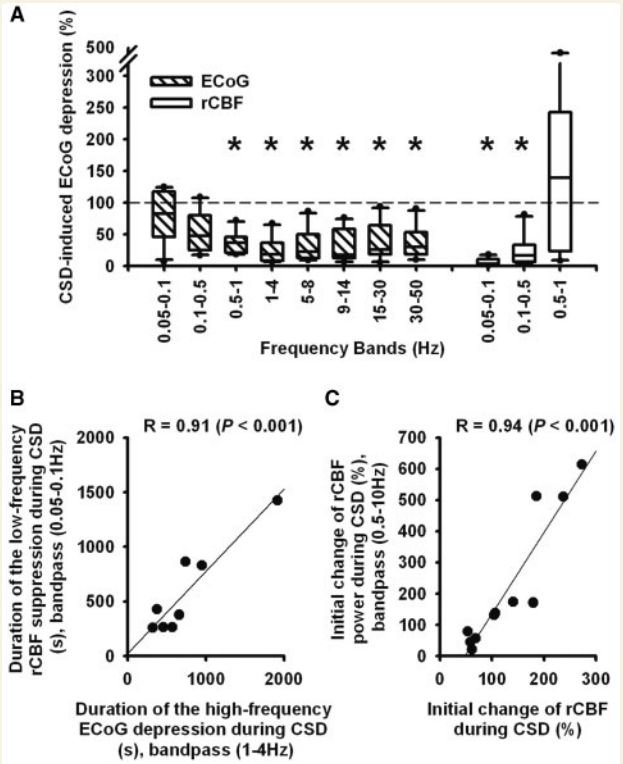

Figure 5 Spreading depression of high-frequency-ECoG activity and spreading suppression of LF-VF correlate in the human brain. (**A**) CSD-induced spreading depression is significant in the high-frequency bands of the ECoG and spreading suppression in the low-frequency bands of regional cerebral blood flow. (**B**) The durations of spreading suppression of LF-VF and spreading depression of high-frequency-ECoG correlate. (**C**) The mean initial change of HF-VF correlates with the mean initial perfusion change in response to CSD. Thus, HF-VF might be a simple measure to estimate the perfusion change in response to CSD using non-invasive recording technology. The findings were similar if the bandwidth of HF-VF was limited to 0.5–2 Hz, more suitable for non-invasive technologies with lower sampling rates.

highly significantly correlated with the mean change in perfusion associated with CSD (Fig. 5C, $R = 0.94$, $P < 0.001$, $n = 12$).

Clusters of recurrent CSDs with prolonged depression of low-frequency vascular fluctuations

Clusters without recovery of high-frequency-ECoG activity between the recurrent CSDs were identified in Cases 1–5. During clusters, all patients were comatose with GCS <6 and ventilated. Three patients were sedated (Table 1). No significant difference was found in vital signs, paraclinical parameters or noradrenaline administration between isolated CSDs and clusters, except that intracranial pressure was significantly higher during clusters [21 (20, 22) versus 17 (16, 18) mmHg, Mann–Whitney Rank Sum Test, $P = 0.031$].

The CSDs contained in a cluster were characterized by a SPC of 2.7 (2.2, 2.7) mV (lower frequency limit: 0.01 Hz). The propagation velocity of CSD was 3.8 (1.6, 4.5) mm/min. The clusters consisted of 6 (5, 8) CSDs that occurred at a median frequency of 2.6 (2.0, 3.6) events/h. Clusters of recurrent CSDs were associated with significant depression of high-frequency-ECoG power. For example in the δ-band, the power significantly decreased from 483 (368, 671) to 64 (55, 76) μV^2 followed by an insignificant recovery to 413 (158, 554) μV^2 (Repeated measures ANOVA on ranks, $P < 0.05$, $n = 5$). The whole depression period lasted for at least 60 h in Case 1. In the remaining four cases, the median depression period was 171 (136, 209) min as assessed for the δ-band.

All clusters contained CSDs associated with inverse haemodynamic response in at least one optode. CSD induced a fall of regional cerebral blood flow to 67 (38, 70)% followed by long-lasting, shallow hyperaemia. Similar to the isolated CSDs, the SPC preceded the initial hypoperfusion by 89 (29, 109) s, indicating that the CSD induced the hypoperfusion and not vice versa. The median duration of the longest CSD-induced initial hypoperfusion contained in a cluster was 24.5 (10.9, 27.7) min. This was significantly longer than the longest CSD-induced initial hypoperfusion measured during isolated CSDs [2.0 (1.5, 4.4) min, Mann–Whitney Rank Sum Test, $P = 0.016$, $n = 5$ in each group].

An example of CSI in a CSD cluster is given in Figs 6 and 7. This CSI occurred in Case 1 on Day 9 after aSAH during a delayed cluster of recurrent, possibly cycling CSDs (Koroleva and Bures, 1979) in presence of the *N*-methyl-D-aspartate (NMDA) receptor antagonist (S)-ketamine at 2 mg/h. The cluster was possibly triggered by hypoglycaemia, since a blood glucose level of 40 mg/dl was measured 2 h and 40 min after the onset. Moreover, TCD and DSA had revealed significant proximal vasospasm. Figure 6A illustrates that the SPC and depression of high-frequency-ECoG activity preceded the onset of the sharp hypoperfusion at optode 4. If the SPC had been the consequence of the regional cerebral blood flow decline, it should have followed the regional cerebral blood flow decline by 2.5–5 min according to previous experimental findings (Leão, 1947). The propagation rate of SPC and regional cerebral blood flow from opto-electrodes 4–5 was 4.9 mm/min (Fig. 6A). Compared with the level at cluster onset, regional cerebral blood flow fell to a minimum value of 6 and 3% at opto-electrodes 4 and 5, respectively; the CSI lasted for 2 h 24 min and 1 h 42 min, respectively. Compared with the CTs of Days 0, 1, 2 and 6 with only oedema, new widespread hypodensities typical of delayed ischaemic infarcts after aSAH were seen on the CT of Day 12 including the recording areas of opto-electrodes 4 and 5 (Fig. 7). After the CSI, the high-frequency-ECoG activity remained depressed at electrodes 3–5, indicating permanent ischaemic loss of neuronal function despite delayed reperfusion (Fig. 7).

$PtiO_2$ was recorded in Cases 1, 4 and 5 during clusters. In all three cases, a progressive sustained reduction of $ptiO_2$ developed from a median value of 24.7–11.4 mmHg with a median recovery to 17.3 mmHg after the cluster.

LF-VF preceded the clusters in only three of five cases. The dominant frequency was 0.063 (0.021, 0.072) Hz. The power of

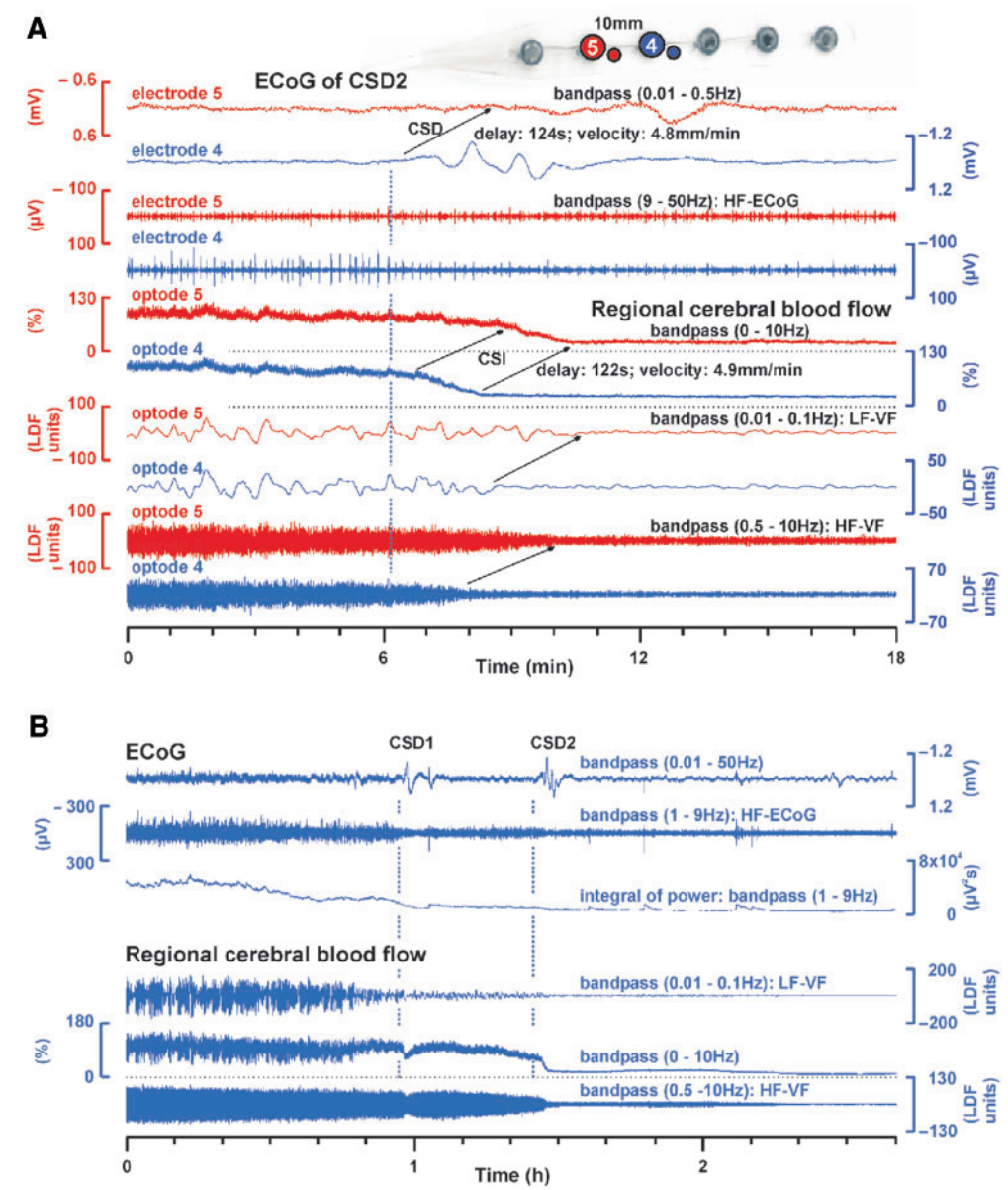

Figure 6 CSI in the human brain (same CSI as in Fig. 7 at higher temporal resolution). (**A**) Note the spreading SPC from electrode 4 (Trace 2, blue) to 5 (Trace 1, red) (velocity of 4.8 mm/min). The onsets of the negative SPC (Trace 2) and depression of the high-frequency-ECoG activity (Trace 4) at electrode 4 clearly preceded the onset of the steep decline of regional cerebral blood flow at optode 4 (Trace 6). If SPC and ECoG depression had been the consequence of the steep regional cerebral blood flow decline, they should have followed it with a delay of 2.5–5 min (Leão, 1947). At opto-electrode 5, the high-frequency-ECoG activity (Trace 3) was already depressed from a previous CSD and the SPC (Trace 1) was rather small. Importantly, the steep decline of regional cerebral blood flow propagated from optode 4 (Trace 6) to 5 (Trace 5) at a characteristic rate of 4.9 mm/min (arrows). The spread was also visible in the suppressions of the LF-VF (traces 7 and 8) and HF-VF (traces 9 and 10). The suppressions of the HF-VF (traces 9 and 10) developed steeply but not in a step-like fashion contrasting other ischaemic aetiologies such as thread occlusion, embolism or cardiac arrest. (**B**) Lower time resolution than (**A**) showing the parallel, progressive suppression of the LF-VF (Trace 4) and depression of the high-frequency-ECoG activity (traces 2 and 3) at opto-electrode 4 during the cluster of CSDs resulting in CSI (Trace 5). Some suppression/depression precedes the appearance of the first SPC (Trace 1) reflected in both LF-VF and high-frequency-ECoG activity. TRACE 6 shows the HF-VF correlating with the changes in level of regional cerebral blood flow.

the LF-VF (bandpass: 0.05–0.1 Hz) decreased from 84.4 (70.9, 1370.3) to 3.4 (2.1, 6.5) LDF U^2 (Fig. 6B) followed by a recovery to 63.4 (32.1, 71.1) LDF U^2 after the cluster. The duration of the depression period of the LF-VF ranged from 211 min to at least 60 h, similar to that of the high-frequency-ECoG activity. As shown in Fig. 6B, the changes of the HF-VF (Trace 6) followed the perfusion changes (Trace 5) during the cluster of recurrent CSDs, as in the case of isolated CSDs.

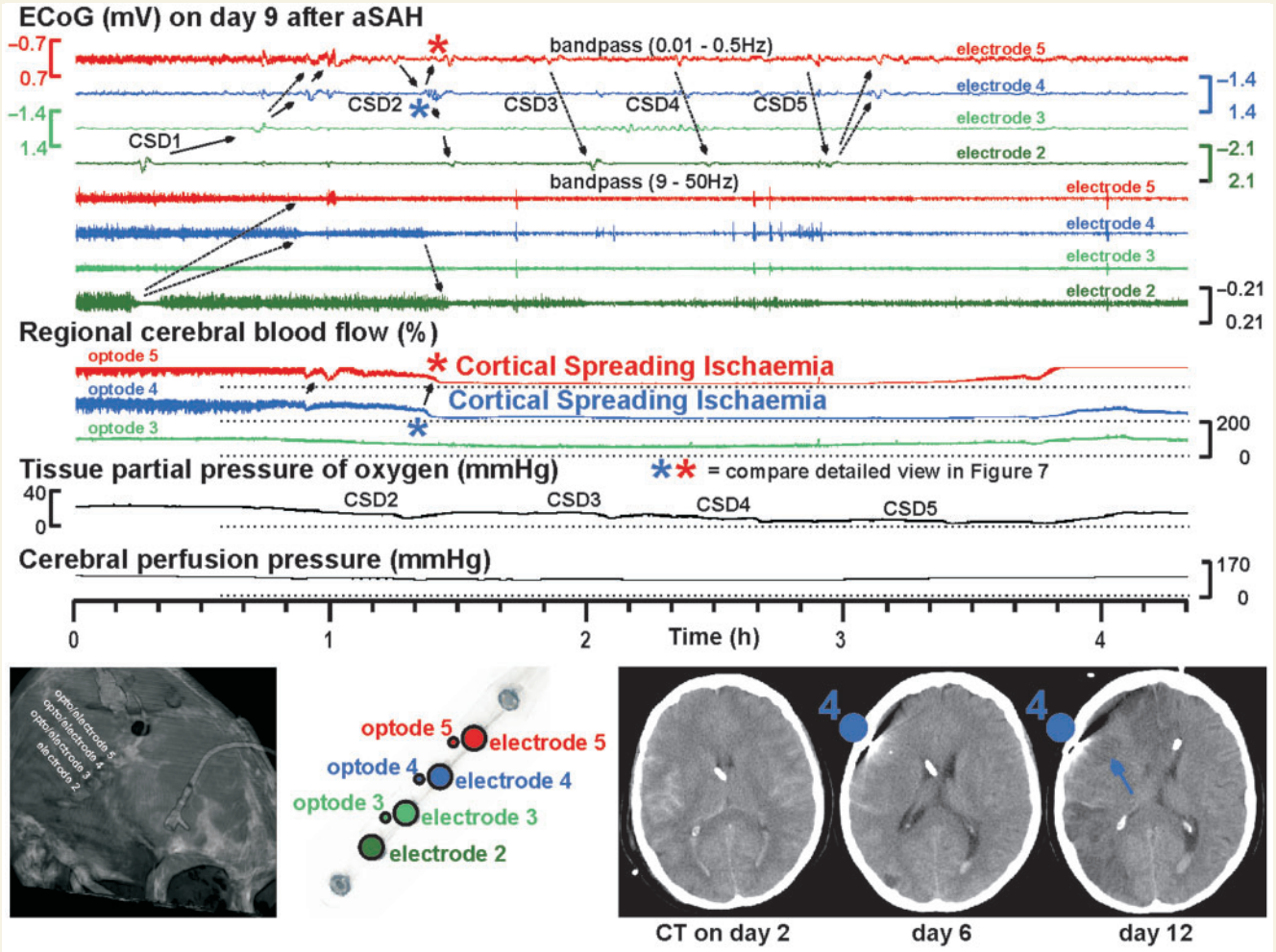

Figure 7 CSI in the human brain (at lower temporal resolution than in Fig. 6). On Day 9, this 62-year-old patient suddenly developed a cluster of CSDs. The position of the original recording strip in relation to the skull is shown in the left lower corner. The upper four traces show the SPCs of electrodes 5–2. The next four traces represent the high-frequency-ECoG activity. Note that the cluster paradoxically started at electrode 2 with only short-lasting depression period and no infarct demarcation in the CT of Day 12. The further complex propagation of the CSDs is illustrated by the arrows. Traces 9–11: regional cerebral blood flow changes at optodes 5–3. The stars indicate the onset of CSI (compare Fig. 6A for higher temporal resolution). Note the long-lasting CSI at optodes 4 and 5 in response to CSD at electrodes 4 and 5. The CSI is accompanied by local decrease of $ptiO_2$ (Trace 12). After CSI the high-frequency-ECoG activity remained depressed at all electrodes apart from electrode 2 (traces 5–8) corresponding with permanent ischaemic loss of neuronal function. Compared to the CTs of Days 2 and 6 with only oedema, the CT of Day 12 showed new hypodensities typical of delayed ischaemic infarcts including the recording areas of opto-electrodes 4 and 5 (right lower corner). This suggested that the recorded hypoperfusion had reached the ischaemic range. The oedema on the CT of Day 6 was already seen on the CTs of Days 0, 1 and 2 suggesting that the initial haemorrhage was the cause. CT cannot differentiate whether the nature of this oedema was vasogenic or cytotoxic. Thus, early ischaemic damage remains a possibility and the images do not provide definitive evidence that the demarcated infarcts on the CT of Day 12 only developed between Days 6 and 12. However, if the tissue had not been viable before the CSI on Day 9, it would not have displayed ECoG activity. Furthermore, a process of infarct demarcation over a period of more than 6 days would be unusual.

Pooled CSDs

Six hundred and three CSDs were recorded in 2467 h recording time in 13 patients. Pooling of all CSDs with simultaneous recordings of regional cerebral blood flow and ECoG (1953 h recording time) resulted in 295 of 417 CSDs with no initial hypoperfusion >30 s, whereas 78 CSDs showed an initial hypoperfusion between 30 s and 2 min, 16 between 2 and 5 min and 28 of >5 min up to 144 min in at least one opto-electrode pair.

Discussion

Using combined invasive recordings of regional cerebral blood flow and regional DC-ECoG, we found that CSDs can be associated with either physiological, absent or inverse haemodynamic responses in the human brain. The regional cerebral blood flow response to CSD effected corresponding $ptiO_2$ changes, suggesting that the haemodynamic response is critical for energy availability during CSD. CSD clusters induced longer CSIs than isolated

CSDs, suggesting that the energy depletion by CSIs contributes to the establishment of such clusters. Spreading suppressions of LF-VF always accompanied spreading depressions of high-frequency-ECoG activity, regardless of the perfusion change. Suppressions of LF-VF persisted for the full duration of depressions of high-frequency-ECoG during CSD clusters. Such clusters were associated with evidence of either early or delayed structural damage on neuroimaging, as reported previously (Dreier *et al*., 2006), and no delayed structural damage occurred in the recording area in the absence of such clusters (Dreier *et al*., 2006).

The negative DC shift of CSD

In the present study, a robust invasive technology was introduced to measure the negative DC potential shift of CSD in the human brain. The invasive DC recordings using polarizable platinum electrodes were remarkably stable, as shown in the figures, and were possible through use of an amplifier without lower frequency limit. In animals, CSD is associated with the largest of all cerebral DC shifts, exceeding that of epileptic seizures by ~10-fold. Here, we found similar amplitudes in the human brain of up to −20 mV. In animals, the negative DC shift of CSD provides an electrophysiological summary measure for the local pathological ion imbalance with net influx of sodium, calcium and water and, thus, for the neuronal injury (Kraig and Nicholson, 1978; Somjen, 2004). Whereas its amplitude reflects the sum of neurons affected, its duration indicates the local cellular capacity to escape from the detrimental cascades initiated by CSD including intracellular sodium and calcium surge, mitochondrial depolarization and extracellular glutamate accumulation that eventually lead to cell death. Of note, whereas CSDs associated with short-lasting DC negativities in healthy tissue are not harmful and are sensitive to NMDA receptor blockers, CSDs associated with longer-lasting DC negativities under pathological conditions become increasingly detrimental and pharmacoresistant due to recruitment of additional cation channels (Müller and Somjen, 1998).

Clinical implications of CSD neuromonitoring

Diffusion-weighted imaging is applied clinically for early detection of the protracted cytotoxic oedema, but is unsuitable to determine online where, when and how the brain makes the transition from health into injury, and from injury into repair (Lo, 2008). However, the electrophysiological signature of CSD has been identified using subdural recording strips for ECoG in patients with traumatic and spontaneous intracerebral haematoma (Fabricius *et al*., 2006). Using subdural ECoG and serial neuroimaging, it has been found that clusters of recurrent CSDs with prolonged depression of high-frequency-ECoG activity were time-locked to the local development of delayed ischaemic stroke after aSAH (Dreier *et al*., 2006). Patients with malignant hemispheric stroke similarly showed a high incidence of clusters of recurrent CSDs with prolonged high-frequency-ECoG depression (Dohmen *et al*., 2008). Thus, it is suggested that monitoring of CSD could be used clinically to differentiate between the phases of lesion progression and repair. This might have profound implications for novel neuroprotective strategies that differentially target such phases (Lo, 2008).

Spreading suppression of LF-VF

The invasiveness of the ECoG recording is a limitation to monitor CSDs in a larger patient population with stroke, hypoxic encephalopathy or traumatic brain injury. The present study suggests that imaging the suppression of LF-VF is a promising candidate to monitor the dynamics of lesion progression in the human brain non-invasively using technology such as functional MRI or near-infrared spectroscopy.

The mechanistic basis for spreading suppression of LF-VF is linked to the term ‘default mode’ that describes the process whereby the brain remains active in an organized fashion during rest (Fox and Raichle, 2007). This concept originates from the finding that some brain regions are more active at rest than during task performance (Raichle *et al*., 2001). CSD provides a depolarization block of the resting neuronal activity, or, in other words, of the ‘default mode’. This block is measured in the ECoG as spreading depression of high-frequency-ECoG activity (Leão *et al*., 1944).

It has been hypothesized that spontaneous fluctuations in the blood oxygen level dependent (BOLD) signal of functional MRI are a manifestation of the ‘default mode’. This hypothesis arose from the coherence of spontaneous BOLD fluctuations recorded in different motor areas in the absence of overt motor behaviour (Biswal *et al*., 1995). The regionally specific BOLD coherence was restricted to frequencies below 0.1 Hz, whereas higher frequencies were related to heart-beat or respiration (Cordes *et al*., 2001).

The BOLD signal mainly reflects local variations in de-oxyhaemoglobin concentration that result from a combination of changes in regional cerebral blood flow and/or oxygen metabolism. Using arterial spin-labelling perfusion MRI, it was shown that low-frequency regionally specific BOLD signal coherences are reflected by similar regionally specific low-frequency coherences of regional cerebral blood flow (De Luca *et al*., 2006). These LF-VF also persist across different resting states, including anaesthesia, indicating that they are an intrinsic property of the brain rather than the result of unconstrained mental activity (Vincent *et al*., 2007).

Our finding that spreading suppression of LF-VF correlated with spreading depression of high-frequency-ECoG activity is consistent with the hypothesis that LF-VF require a neuronal input. Alternatively, LF-VF could originate from ‘vasomotion’, i.e. an oscillation generated from within the vascular wall without neuronal input. ‘Vasomotion’ could be blocked by CSD (Piper *et al*., 1991) if the extracellular changes somehow interfere with the gap junction communication between vascular smooth muscle cells. However, this is contradicted by the finding that vascular conduction is preserved in mice and rats during CSD (Brennan *et al*., 2007). Moreover, cellular swelling could act mechanically as a high-pass filter on the microvascular walls during CSD, thereby blocking ‘vasomotion’ in contrast to HF-VF. However, the depression periods of the LF-VF were too long in relation to the measured DC negativities for this mechanism: extracellular

volume changes outlast DC negativities by at most 50% in animals (Windmüller *et al*., 2005). Furthermore, (i) 'vasomotion' is typically enhanced by vasoconstriction (Nilsson and Aalkjær, 2003); and (ii) Schmidt reviewed the question of whether 'vasomotion' occurs at all under physiological conditions and concluded that 'vasomotion' is primarily associated with ischaemic conditions in various vascular beds (Schmidt, 1996). Thus, the suppression of the LF-VF during CSI in the present study strongly contrasts the typical behaviour of 'vasomotion'. Thus, whether LF-VF in the brain are due to 'vasomotion' or require a neuronal input cannot be conclusively answered, but our findings strongly support the latter (Fox and Raichle, 2007).

HF-VF might be used to estimate the perfusion response to CSD non-invasively

Pressure and flow amplitudes of the arterial pulse decay along the branching arterial tree (Gross *et al*., 1974). This decay of microvascular pulsatility in the high-frequency range is dependent on the resistance of upstream arterioles. The lower the vascular tone in upstream arterioles, the higher the downstream high-frequency pulsatility and vice versa. Consistently, in contrast to LF-VF, the HF-VF amplitude changed in accordance with perfusion changes associated with CSD.

The physiological haemodynamic response to CSD

The physiological haemodynamic response to CSD is characterized by the hyperperfusion associated with the negative cortical DC shift followed by a mild hypoperfusion after recovery of the DC potential. A body of evidence indicates that CSD is primarily a phenomenon of neurons rather than astrocytes (Basarsky *et al*., 1998; Peters *et al*., 2003; Somjen, 2004). Hence, the physiological haemodynamic response to CSD seems to result from a coupling process between neurons and vasculature. Classically, the term neurovascular coupling describes the increased regional cerebral blood flow in response to neuronal activation and decreased regional cerebral blood flow in response to neuronal inhibition (Devor *et al*., 2007). It is increasingly recognized that neurotransmitter and neuropeptide release during synaptic transmission is a major contributor to the neurovascular response (Attwell and Iadecola, 2002; Hamel, 2006). Neural activation leads to glutamate-evoked calcium influx in postsynaptic neurons that activates production of NO and arachidonic acid metabolites. The resulting vasodilatation reflects both the presynaptic activity and the level of postsynaptic depolarization, which changes the magnesium block of NMDA receptors and the resulting influx of calcium (Attwell and Iadecola, 2002).

The physiological haemodynamic response to CSD seems to conflict with this classical definition of neurovascular coupling, since an increased regional cerebral blood flow is coupled to depression of neuronal activity. This paradox is resolved by the fact that activity depression during CSD results from a depolarization block of action potential generation. Spreading depression of high-frequency-ECoG thus reflects a form of intense excitation, in contrast to neuronal inhibition resulting from GABA-mediated hyperpolarization. CSD shares several additional features in common with neuronal excitation and in contrast with inhibition: (i) glutamate is markedly released and, thus, vasoeffectors such as NO are released as well (Busija *et al*., 2008); (ii) although the ion concentration changes during CSD are markedly higher, the direction of ion fluxes is similar to that during neuronal excitation and their net effect is vasodilatation (Windmüller *et al*., 2005) and (iii) metabolism and energy demand are increased during CSD (Mies and Paschen, 1984; Gault *et al*., 1994). Thus, the physiological response of hyperaemia to CSD is consistent with other forms of normal neurovascular coupling to depolarization such as during physiological activation or epileptic activity, despite the fact that the neuronal excitation during CSD is so intense that even the ability for action potential generation is lost. As in previous experimental publications on CSI (Dreier *et al*., 2002; Petzold *et al*., 2003, 2005; Windmüller *et al*., 2005), we have used the term 'inverse' haemodynamic response to describe hypoperfusion associated with the depolarization phase of CSD since the normal mechanisms coupling neuronal depolarization, glutamate release and increased energy demand to increased regional cerebral blood flow are impaired such that they produce the inverse effect.

The inverse haemodynamic response to CSD

We found clear evidence of inverse haemodynamic responses to CSD in our patients: the hypoperfusion was coupled to the prolonged negative DC shift followed by hyperperfusion after recovery of the DC potential. CSI showed a continuous spectrum of up to 144 min duration, as in previous animal studies (Dreier *et al*., 2000; Shin *et al*., 2006; Strong *et al*., 2007). Experimental evidence suggests that the enormous prolongation of the CSD-induced initial hypoperfusion is the result of a vicious cycle between neuronal release of vasoconstrictors such as potassium, the reduced supply and increased demand for ATP, and the consequent failure of the sodium pump. This latter prevents clearance of the vasoconstrictor potassium from the extracellular space and thus maintains the hypoperfusion (Dreier *et al*., 2002; Sukhotinsky *et al*., 2008).

Possible contributors to inverse haemodynamic responses after aSAH have been discussed previously (Dreier *et al*., 2000). Briefly, proximal vasospasm might contribute to CSI in analogy to the penumbra after MCA occlusion (Shin *et al*., 2006; Strong *et al*., 2007). The NO scavenging effect of haemoglobin in the clot, endogenous NOS inhibitors or degeneration of perivascular nitrergic nerves might play a role (Dreier *et al*., 1998; MacDonald *et al*., 2007) as well as astrocyte-mediated vasoconstriction (Mulligan and MacVicar, 2004; Tomita *et al*., 2005; Chuquet *et al*., 2007), increased baseline potassium (Dreier *et al*., 2000), endothelin-1 (Petzold *et al*., 2003) and rho-kinase (Shin *et al*., 2007). ICP was significantly higher during clusters of recurrent CSDs than during isolated CSDs in our patients. It deserves further study

whether elevated intracranial pressure promotes the occurrence of clusters and CSI.

Possible interventions targeting CSI

Interestingly, the CSD cluster associated with CSI in Case 1 was not prevented by the NMDA receptor antagonist (S)-ketamine, which is consistent with previous animal findings (Petzold *et al*., 2005).

All patients were treated prophylactically with nimodipine (Pickard *et al*., 1989; Dorhout *et al*., 2008). Experimental evidence has suggested that this L-type calcium antagonist causes CSI to revert to a more physiological haemodynamic response to CSD and, thus, may protect the brain (Dreier *et al*., 1998; Windmüller *et al*., 2005). However, the dose is limited by systemic side-effects and this might explain why CSIs occurred despite the presence of nimodipine. Possibly, surgical placement of drug-containing prolonged-release implants at the basal cerebral arteries provide a better treatment option, since proximal vasospasm is prevented more effectively and the cerebrospinal fluid circulation might transport the drug over the hemispheric surface where microvascular spasm and CSI are targeted (Barth *et al*., 2007).

Cerebral glucose may be another target for intervention. Hyperglycaemia has been associated with worse outcome after ischaemic stroke (Mohr *et al*., 1985). However, while glycaemic control with insulin has been established in intensive care patients in general surgery (van den Berghe *et al*., 2001), translation of this concept into improved clinical management of acute stroke has failed so far (Gray *et al*., 2007). Specifically in aSAH patients, significant associations of low cerebral glucose with unfavourable outcome and severe cellular distress have been found recently (increases in lactate/pyruvate ratio, glutamate and glycerol as measured by cerebral microdialysis) (Schlenk *et al*., 2008). In the present study, insulin treatment in Case 1 was associated with a hypoglycaemic episode that was time-locked to, and possibly triggered, the delayed cluster of recurrent CSDs and CSI on Day 9 after the initial haemorrhage. In the ischaemic penumbra in animals, even mild reduction in plasma glucose has been associated with increased frequency of CSDs (Strong *et al*., 2000), whilst superfusion of the cortex with solution containing haemoglobin and low-glucose-induced CSI (Dreier *et al*., 2000). These findings call for a clinical study on glycaemic control after aSAH to determine the optimal range of plasma glucose. In such a trial the assessment of patient outcome should be complemented by the monitoring of ECoG, regional cerebral blood flow, $ptiO_2$ and metabolism.

Moreover, blockade of chronic vasospasm remains an important therapeutic objective. Neuromonitoring in a randomized clinical trial of the endothelin antagonist clazosentan could help us to understand the possible links between chronic vasospasm and CSI as well as their relative contributions to ischaemic damage and patient outcome after aSAH (MacDonald *et al*., 2007). We should consider the possibility that only combination therapies targeting vasospasm, disturbed neuronal function and disturbed neurovascular coupling might improve patient outcome significantly.

Conclusion

This translational study has established proof of CSI as a novel pathophysiological mechanism of disease and potential target for neuroprotective intervention in the human brain. Moreover, imaging the spreading suppression of LF-VF is suggested as a promising tool to differentiate between progressive ischaemic damage and repair phases in the human brain non-invasively.

Funding

Deutsche Forschungsgemeinschaft (DFG DR 323/3-1, 323/5-1); Bundesministerium für Bildung und Forschung (Center for Stroke Research Berlin, 01 EO 0801); Kompetenznetz Schlaganfall (to J.P.D.); Novo Nordisk Foundation (to M.F.); Lundbeck Foundation Center for Neurovascular Signalling (to M.L.); HeadFirst (to A.J.S.).

References

Attwell D, Iadecola C. The neural basis of functional brain imaging signals. Trends Neurosci 2002; 25: 621–5.

Back T, Kohno K, Hossmann KA. Cortical negative DC deflections following middle cerebral artery occlusion and KCl-induced spreading depression: effect on blood flow, tissue oxygenation, and electroencephalogram. J Cereb Blood Flow Metab 1994; 14: 12–9.

Barth M, Capelle HH, Weidauer S, Weiss C, Münch E, Thomé C, et al. Effect of nicardipine prolonged-release implants on cerebral vasospasm and clinical outcome after severe aneurysmal subarachnoid hemorrhage: a prospective, randomized, double-blind phase IIa study. Stroke 2007; 38: 330–6.

Basarsky TA, Duffy SN, Andrew RD, MacVicar BA. Imaging spreading depression and associated intracellular calcium waves in brain slices. J Neurosci 1998; 18: 7189–99.

Biswal B, Yetkin FZ, Haughton VM, Hyde JS. Functional connectivity in the motor cortex of resting human brain using echo-planar MRI. Magn Reson Med 1995; 34: 537–41.

Brennan KC, Beltrán-Parrazal L, López-Valdés HE, Theriot J, Toga AW, Charles AC. Distinct vascular conduction with cortical spreading depression. J Neurophysiol 2007; 97: 4143–51.

Busija DW, Bari F, Domoki F, Horiguchi T, Shimizu K. Mechanisms involved in the cerebrovascular dilator effects of cortical spreading depression. Prog Neurobiol 2008; 86: 379–95.

Chuquet J, Hollender L, Nimchinsky EA. High-resolution in vivo imaging of the neurovascular unit during spreading depression. J Neurosci 2007; 27: 4036–44.

Cordes D, Haughton VM, Arfanakis K, Carew JD, Turski PA, Moritz CH, et al. Frequencies contributing to functional connectivity in the cerebral cortex in ''resting-state'' data. AJNR Am J Neuroradiol 2001; 22: 1326–33.

De Luca M, Beckmann CF, De Stefano N, Matthews PM, Smith SM. fMRI resting state networks define distinct modes of long-distance interactions in the human brain. Neuroimage 2006; 29: 1359–67.

Devor A, Tian P, Nishimura N, Teng IC, Hillman EM, Narayanan SN, et al. Suppressed neuronal activity and concurrent arteriolar vasoconstriction may explain negative blood oxygenation level-dependent signal. J Neurosci 2007; 27: 4452–9.

Dohmen C, Sakowitz OW, Fabricius M, Bosche B, Reithmeier T, Ernestus RI, et al. Spreading depolarizations occur in human ischemic stroke with high incidence. Ann Neurol 2008; 63: 720–8.

Dorhout Mees SM, Rinkel GJ, Feigin VL, Algra A, van den Bergh WM, Vermeulen M, et al. Calcium antagonists for aneurysmal subarachnoid hemorrhage. Stroke 2008; 39: 514.

Dreier JP, Körner K, Ebert N, Görner A, Rubin I, Back T, et al. Nitric oxide scavenging by hemoglobin or nitric oxide synthase inhibition by N-nitro-L-arginine induces cortical spreading ischemia when K^+ is increased in the subarachnoid space. J Cereb Blood Flow Metab 1998; 18: 978–90.

Dreier JP, Ebert N, Priller J, Megow D, Lindauer U, Klee R, et al. Products of hemolysis in the subarachnoid space inducing spreading ischemia in the cortex and focal necrosis in rats: a model for delayed ischemic neurological deficits after subarachnoid hemorrhage? J. Neurosurg 2000; 93: 658–66.

Dreier JP, Windmüller O, Petzold G, Lindauer U, Einhäupl KM, Dirnagl U. Ischemia caused by inverse coupling between neuronal activation and cerebral blood flow in rats. In: Tomita M, Kanno I, Hamel E, editors. Brain activation and CBF control. Amsterdam: Elsevier; 2002. p. 487–92.

Dreier JP, Woitzik J, Fabricius M, Bhatia R, Major S, Drenckhahn C, et al. Delayed ischaemic neurological deficits after subarachnoid haemorrhage are associated with clusters of spreading depolarizations. Brain 2006; 129: 3224–37.

Fabricius M, Fuhr S, Bhatia R, Boutelle M, Hashemi P, Strong AJ, et al. Cortical spreading depression and peri-infarct depolarization in acutely injured human cerebral cortex. Brain 2006; 129: 778–90.

Fox MD, Raichle ME. Spontaneous fluctuations in brain activity observed with functional magnetic resonance imaging. Nat Rev Neurosci 2007; 8: 700–11.

Gault LM, Lin CW, LaManna JC, Lust WD. Changes in energy metabolites, cGMP and intracellular pH during cortical spreading depression. Brain Res 1994; 641: 176–80.

Gray CS, Hildreth AJ, Sandercock PA, O'Connell JE, Johnston DE, Cartlidge NE, et al. Glucose-potassium-insulin infusions in the management of post-stroke hyperglycaemia: the UK Glucose Insulin in Stroke Trial (GIST-UK). Lancet Neurol 2007; 6: 397–406.

Gross JF, Intaglietta M, Zweifach BW. Network model of pulsatile hemodynamics in the microcirculation of the rabbit omentum. Am J Physiol 1974; 226: 1117–23.

Hamel E. Perivascular nerves and the regulation of cerebrovascular tone. J Appl Physiol 2006; 100: 1059–64.

Klatzo I. Pathophysiological aspects of brain edema. Acta Neuropathol 1987; 72: 236–39.

Koroleva VI, Bures J. Circulation of cortical spreading depression around electrically stimulated areas and epileptic foci in the neocortex of rats. Brain Res 1979; 173: 209–15.

Kraig RP, Nicholson C. Extracellular ionic variations during spreading depression. Neuroscience 1978; 3: 1045–59.

Lauritzen M. Pathophysiology of the migraine aura. The spreading depression theory. Brain 1994; 117: 199–210.

Leão AAP. Spreading depression of activity in the cerebral cortex. J Neurophysiol 1944; 7: 359–90.

Leão AAP. Further observations on the spreading depression of activity in the cerebral cortex. J Neurophysiol 1947; 10: 409–14.

Leopold DA, Murayama Y, Logothetis NK. Very slow activity fluctuations in monkey visual cortex: implications for functional brain imaging. Cereb Cortex 2003; 13: 422–33.

Lo EH. A new penumbra: transitioning from injury into repair after stroke. Nat Med 2008; 14: 497–500.

Macdonald RL, Pluta RM, Zhang JH. Cerebral vasospasm after subarachnoid hemorrhage: the emerging revolution. Nat Clin Pract Neurol 2007; 3: 256–63.

Mies G, Paschen W. Regional changes of blood flow, glucose, and ATP content determined on brain sections during a single passage of spreading depression in rat brain cortex. Exp Neurol 1984; 84: 249–58.

Mohr JP, Rubinstein L, Edelstein SZ, Gross CR, Heyman A, Kase CS, et al. Approaches to pathophysiology of stroke through the NINCDS Data Bank. In: Plum F, Pulsinelli WA, editors. Cerebrovascular diseases (Fourteenth Research Conference). New York: Raven; 1985. p. 63–8.

Müller M, Somjen GG. Inhibition of major cationic inward currents prevents spreading depression-like hypoxic depolarization in rat hippocampal tissue slices. Brain Res 1998; 812: 1–13.

Mulligan SJ, MacVicar BA. Calcium transients in astrocyte endfeet cause cerebrovascular constrictions. Nature 2004; 431: 195–9.

Nedergaard M, Hansen AJ. Characterization of cortical depolarizations evoked in focal cerebral ischemia. J Cereb Blood Flow Metab 1993; 13: 568–74.

Nilsson H, Aalkjaer C. Vasomotion: mechanisms and physiological importance. Mol Interv 2003; 3: 79–89.

Peters O, Schipke CG, Hashimoto Y, Kettenmann H. Different mechanisms promote astrocyte Ca^{2+} waves and spreading depression in the mouse neocortex. J Neurosci 2003; 23: 9888–96.

Petzold GC, Einhäupl KM, Dirnagl U, Dreier JP. Ischemia triggered by spreading neuronal activation is induced by endothelin-1 and hemoglobin in the subarachnoid space. Ann Neurol 2003; 54: 591–8.

Petzold GC, Windmüller O, Haack S, Major S, Buchheim K, Megow D, et al. Increased extracellular K^+ concentration reduces the efficacy of N-methyl-D-aspartate receptor antagonists to block spreading depression-like depolarizations and spreading ischemia. Stroke 2005; 36: 1270–7.

Pickard JD, Murray GD, Illingworth R, Shaw MD, Teasdale GM, Foy PM, et al. Effect of oral nimodipine on cerebral infarction and outcome after subarachnoid haemorrhage: British aneurysm nimodipine trial. Br Med J 1989; 298: 636–42.

Piper RD, Lambert GA, Duckworth JW. Cortical blood flow changes during spreading depression in cats. Am J Physiol 1991; 261: H96–102.

Raichle ME, MacLeod AM, Snyder AZ, Powers WJ, Gusnard DA, Shulman GL. A default mode of brain function. Proc Natl Acad Sci USA 2001; 98: 676–82.

Schlenk F, Nagel A, Graetz D, Sarrafzadeh AS. Hyperglycemia and cerebral glucose in aneurysmal subarachnoid hemorrhage. Intensive Care Med 2008; 34: 1200–7.

Schmidt JA. Periodic hemodynamics in health and disease. Heidelberg: Springer; 1996.

Shin HK, Dunn AK, Jones PB, Boas DA, Moskowitz MA, Ayata C. Vasoconstrictive neurovascular coupling during focal ischemic depolarizations. J Cereb Blood Flow Metab 2006; 26: 1018–30.

Shin HK, Salomone S, Potts EM, Lee SW, Millican E, Noma K, et al. Rho-kinase inhibition acutely augments blood flow in focal cerebral ischemia via endothelial mechanisms. J Cereb Blood Flow Metab 2007; 27: 998–1009.

Somjen GG. Ions in the brain. Normal function, seizures and stroke. New York: Oxford University Press; 2004.

Strong AJ, Anderson PJ, Watts HR, Virley DJ, Lloyd A, Irving EA, et al. Peri-infarct depolarizations lead to loss of perfusion in ischaemic gyrencephalic cerebral cortex. Brain 2007; 130: 995–1008.

Strong AJ, Smith SE, Whittington DJ, Meldrum BS, Parsons AA, Krupinski J, et al. Factors influencing the frequency of fluorescence transients as markers of peri-infarct depolarizations in focal cerebral ischaemia. Stroke 2000; 31: 214–22.

Sukhotinsky I, Dilekoz E, Moskowitz MA, Ayata C. Hypoxia and hypotension transform the blood flow response to cortical spreading depression from hyperemia into hypoperfusion in the rat. J Cereb Blood Flow Metab 2008; 28: 1369–76.

Tomita M, Schiszler I, Tomita Y, Tanahashi N, Takeda H, Osada T, et al. Initial oligemia with capillary flow stop followed by hyperemia during K^+-induced cortical spreading depression in rats. J Cereb Blood Flow Metab 2005; 25: 742–7.

van den Berghe G, Wouters P, Weekers F, Verwaest C, Bruyninckx F, Schetz M, et al. Intensive insulin therapy in the critically ill patients. N Engl J Med 2001; 345: 1359–67.

Vincent JL, Patel GH, Fox MD, Snyder AZ, Baker JT, Van Essen DC, et al. Intrinsic functional architecture in the anaesthetized monkey brain. Nature 2007; 447: 83–6.

Windmüller O, Lindauer U, Foddis M, Einhäupl KM, Dirnagl U, Heinemann U, et al. Ion changes in spreading ischaemia induce rat middle cerebral artery constriction in the absence of NO. Brain 2005; 128: 2042–51.